

Self-Supervised Reversed Image Signal Processing via Reference-Guided Dynamic Parameter Selection

Junji Otsuka Masakazu Yoshimura Takeshi Ohashi
Sony Group Corporation

{junji.otsuka, masakazu.yoshimura, takeshi.a.ohashi}@sony.com

Abstract

Unprocessed sensor outputs (RAW images) potentially improve both low-level and high-level computer vision algorithms, but the lack of large-scale RAW image datasets is a barrier to research. Thus, reversed Image Signal Processing (ISP) which converts existing RGB images into RAW images has been studied. However, most existing methods require camera-specific metadata or paired RGB and RAW images to model the conversion, and they are not always available. In addition, there are issues in handling diverse ISPs and recovering global illumination. To tackle these limitations, we propose a self-supervised reversed ISP method that does not require metadata and paired images. The proposed method converts a RGB image into a RAW-like image taken in the same environment with the same sensor as a reference RAW image by dynamically selecting parameters of the reversed ISP pipeline based on the reference RAW image. The parameter selection is trained via pseudo paired data created from unpaired RGB and RAW images. We show that the proposed method is able to learn various reversed ISPs with comparable accuracy to other state-of-the-art supervised methods and convert unknown RGB images from COCO and Flickr1M to target RAW-like images more accurately in terms of pixel distribution. We also demonstrate that our generated RAW images improve performance on real RAW image object detection task.

1. Introduction

In general, a sensor RAW image taken by a digital camera is converted into the standard RGB (sRGB) format through an in-camera ISP [20]. Traditional ISPs are essentially optimized to generate compressed and human perceptually pleasant RGB images. Due to the ease of use, numerous RGB images flood on the Internet, and their availability underpin recent advance in machine learning-based computer vision technologies. On the other hand, RAW images contain all the captured information, and the rela-

tionship between ambient light, pixel intensity, and noise distribution in RAW domain is much simpler than that in RGB domain [50]. Therefore, utilizing RAW images directly for downstream tasks potentially achieves greater performance than RGB image-based methods in both low-level and high-level computer vision tasks. In fact, recent studies have shown that RAW image-based image recognition [36, 15, 49] and image processing [3, 53, 54, 28] achieved higher performance than RGB image-based methods. The use of RAW images is expected to improve performance especially in difficult scenes such as extremely dark or blurry scenes that should be covered in practical application. RAW images are also used in research that optimizes existing ISPs for downstream tasks [40, 37, 13, 38, 46, 42, 52] or develops an accurate DNN-based ISP [31, 44, 17]. However, they are hard-to-see and not suitable for daily use. Therefore, it is difficult to obtain enough RAW images for research purposes. In particular, the scarcity of annotated RAW data has been a barrier to machine learning-based approaches. Hence, several reversed ISP methods that convert existing large-scale RGB datasets into pseudo RAW datasets have been studied [3, 53, 7, 47, 8, 22, 2].

The reversed ISP methods can be divided into model-based methods [22, 3] and learning-based methods [53, 7, 47, 2, 8]. UPI [3] is a typical model-based method that defines a series of simple and invertible ISP blocks whose parameters are determined using camera metadata such as white balance gains and color correction matrixes. On the other hand, learning-based methods learn RGB-to-RAW conversion directly from paired RGB and RAW images using a fully DNN based model [53, 2, 47, 8] or a combination of hand-crafted ISP blocks and shallow CNN models [7, 8]. Learning-based methods are able to achieve more accurate RAW reconstruction than model-based methods.

These methods are pioneers of reversed ISP research and valuable to overcome the shortage of RAW images. However, there are some limitations. First, camera metadata or paired RAW and RGB data is required. Metadata is often not accessible for camera users, and shooting RGB and RAW images simultaneously is not executable in all cases.

Second, most existing methods assume a single specific ISP pipeline and do not handle RGB images processed by unknown ISP well. This causes misaligned color and brightness distribution when applied to arbitrary RGB datasets. Finally, it is hard to reproduce characteristics of global illumination of a target RAW image from an input RGB image since the effect of global illumination is generally canceled in RGB images by ISPs. Therefore, the existing methods tend to produce different RAW image distribution from the target distribution.

To tackle these problems, in this paper, we present a Self-supervised Reversed ISP method called SRISP that does not require metadata and paired data for training. Same as MBISPLD [7], SRISP has multiple parameter dictionaries of a reversed ISP pipeline composed of classical ISP functions and shallow CNNs to cover various kinds of sensors and environments. Then, the parameters are selected by other shallow CNNs to achieve correct mapping. Unlike MBISPLD, the proposed method (1) only needs source RGB images and unpaired target RAW images to train it with the help of proposed two types of pseudo image pairs and (2) achieves diverse RGB-to-RAW mapping including illumination effects by conditioning the selection module with global features of reference target RAW and source RGB images. Our main contributions are:

- Self-supervised reversed ISP learning based on two types of pseudo paired data generated from unpaired target RAW and source RGB images using a randomized traditional ISP and novel self-supervision based on Mean Teacher [45].
- Dynamic parameter selection of reversed ISP blocks using global features of a reference RAW image, which is able to reproduce the target RAW characteristic including global illumination.
- Demonstrate that our method is able to map existing RGB datasets (COCO [29] and Flickr1M [35]) to target RAW datasets (MIT-Adobe FiveK [5], SIDD [1], and LOD Dataset [15]) more accurately than other state-of-the-art methods in terms of pixel distribution.
- Additional experiments that show our learned model contributes to the accuracy improvement in RAW object detection on LOD Dataset.

2. Relate Work

2.1. Reversed ISP

The learning-based methods are further divided into fully DNN-based methods [53, 2, 47, 8, 25, 10, 56, 21] and hybrid-methods [7, 8]. CycleISP [53] and InvISP [47] are state-of-the-art fully DNN-based methods. CycleISP models RGB-to-RAW and RAW-to-RGB mappings using two DNN branches that are jointly fine-tuned to achieve cycle

consistency. InvISP learns a reversible ISP using normalizing flow [24, 14] to produce an invertible RGB image to the original RAW image. While the fully DNN-based methods are expressive, there are issues of interpretability and controllability. On the other hand, MBISPLD [7] employs a hybrid approach combining UPI-like classical reversible ISP blocks and shallow CNNs. Each ISP block has learnable parameters optimized with RGB and RAW image pairs. As for the white balance and color correction blocks, multiple candidate parameters (parameter dictionary) are learned and dynamically selected by shallow CNNs based on intermediate images at inference time. They also use shallow CNNs as the learnable lens shading correction and tone mapping. MBISPLD achieved state-of-the-art RAW reconstruction accuracy while maintaining the interpretability. Our method is an extension of MBISPLD, which is composed of classic ISP blocks and shallow CNNs. The main differences are the parameter selection module and the self-supervised learning method. Our method selects optimal parameters of ISP blocks based on global features of source and reference images and is end-to-end trainable with unpaired RGB and RAW images.

2.2. ISP Optimization and Control

Recently, several methods have been proposed to optimize parameters of a classic ISP to improve the performance of downstream tasks or perceptual image quality [40, 37, 13, 38, 46, 42, 52]. For example, in [46], the differentiable proxy that mimics the behavior of a non-differentiable ISP function using DNN is trained, and the ISP parameters are optimized based on the proxy directly using gradient descent to maximize performance of several downstream tasks. Similarly, Covariance Matrix Adaptation Evolution Strategy [12] is used to optimize black-box ISP parameters [37]. In addition, ReconfigISP [4] optimizes both the combination of ISP blocks and their parameters with a neural architecture search method [30]. Unlike these static ISP optimization, several methods [39, 49, 36, 9] dynamically control ISP parameters such as the digital gain, white balance, denoiser, and tone mapping to enhance the downstream performance. These studies show that even a model-based ISP with limited expressiveness achieves high performance by optimizing or controlling its parameters.

2.3. Pseudo Labeling

In the field of image recognition, pseudo-labeling that treats outputs of a specific model (teacher) as ground truth data is widely used when the real ground truth data is not available or noisy. In particular, Mean Teacher (MT) [45], which uses an Exponential Moving Average (EMA) model of past training step models as a teacher, has been shown to be effective in self-supervised learning, semi-supervised learning, and domain adaptation in recent years

[26, 27, 32, 33]. MT suppresses the error of the pseudo-labels by the temporal model ensemble and is expected to achieve stable training. In this study, we propose a MT-based pseudo-paired data generation method for better training.

3. Method

Figure 1 shows an overview of our proposed approach. Let us denote \mathcal{X} as RGB image domain and \mathcal{Y} as RAW image domain. Our goal is to find the reversed mapping $f^{-1} : \mathcal{X} \rightarrow \mathcal{Y}$. Similar to UPI [3] and MBISPLD [7], we modeled the mapping function by a series of differentiable and reversible ISP blocks: Global Gain (GG) f_{gg} , White Balance (WB) f_{wb} , Color Correction (CC) f_{cc} , Gamma Correction (GC) f_{gc} , and Tone Mapping (TM) f_{tm} . Note that bilinear demosaicing is applied before f_{gg} as preprocessing because it is deterministic processing, and the demosaiced image is treated as a RAW image in this paper. The RGB-to-RAW mapping f^{-1} is defined as follows:

$$f^{-1} = f_{gg}^{-1} \circ f_{wb}^{-1} \circ f_{cc}^{-1} \circ f_{gc}^{-1} \circ f_{tm}^{-1}. \quad (1)$$

The i -th ISP block has a parameter dictionary D_{θ_i} with K parameter candidates $\{\theta_{i,k}\}_{k=1\dots K}$. The final parameter θ_i of the i -th block is determined by a Dynamic Parameter Selector (DPS) f_{DPS} based on the parameter dictionary so that a given RGB image x is converted into a corresponding RAW image y . However, in general, if the functions and parameters of the forward mapping are unknown, the inversion estimation is ill-posed as there can be many RAW images corresponding to an input RGB image. It is hard to estimate what true illumination was and how the RGB image was processed from only the input RGB image since their clues are essentially removed by a forward ISP. Therefore, we solve this problem by giving a reference RAW image y_r to the DPS. Then, the proposed method is able to convert x processed by an arbitrary ISP into a y_r -like RAW image y . Furthermore, the parameter dictionaries and the DPS are trained using unpaired RGB and RAW images.

We implemented GG, WB, CC, and GC based on UPI. Due to space limitation, we detail them in the supplementary material. The key point is, while MBISPLD unifies CG into WB with a single parameter dictionary, we designed them separately with independent dictionaries to enhance their flexibility. As for TM, we introduced new Dynamic Tone Mapping (DTM) described in Section 3.2.

3.1. Dynamic Parameter Selector

Following MBISPLD, we designed our DPS to estimate the parameter θ_i of the i -th ISP block as a weighted average of the parameter dictionary D_{θ_i} as follows:

$$\theta_i = \sum_{k=1}^K w_{i,k} \theta_{i,k}. \quad (2)$$

Unlike MBISPLD, our model attempts to map an input RGB image x to a RAW-like image y similar to reference RAW image y_r . To this end, the weights $w_i = \{w_{i,k}\}_{k=1\dots K}$ are determined by Reference-guided Weight Estimator (RWE) f_{RWE} based on 1D global features $g_x = h_x(x)$, $g_r = h_r(y_r)$, and $g_i = h_i(\tilde{x}_i)$:

$$w_i = f_{RWE}(g_x, g_r, g_i), \quad (3)$$

where h_x , h_r , and h_i are shallow CNNs followed by the global average pooling, and \tilde{x}_i is intermediate features of the i -th ISP block. For the blocks except for the DTM, following MBISPLD, \tilde{x}_i is the concatenated output image processed by the ISP block using the K parameter candidates. As for the DTM, the input image x is used as \tilde{x}_i to avoid heavy computation. As shown in Figure 2, the f_{RWE} simply fuses the three global features using affine layers ($f_{x \rightarrow r}$, $f_{prj,i}$, and $f_{head,i}$) and element-wise sum operations, and outputs w_i with a softmax operation. The $f_{x \rightarrow r}$ is shared for all ISP blocks and generates the fused global feature $g_{x \rightarrow r}$ of g_x and g_r . The $g_{x \rightarrow r}$ is expected to represent general information how to convert x to y_r . The $f_{prj,i}$ and $f_{head,i}$ are trained for each parameter dictionary and select suitable parameters based on $g_{x \rightarrow r}$ and g_i . Thanks to $g_{x \rightarrow r}$, our method is able to reproduce features of the reference RAW image and generate diverse pseudo RAW images using y_r randomly sampled from the target RAW data. Note that a full-resolution image is firstly resized to 256×256 , and ISP parameters are determined based on the resized image to reduce a computational cost. Then, the full-resolution image is processed using the parameters.

3.2. Dynamic Tone Mapping

The tone mapping maps one color to another color to render a perceptually pleasant image, and the mapping function can be highly complex. To model the complex mapping, we employed a shallow CNN as TM similar to MBISPLD:

$$f_{tm}(x, \theta_1) = \phi_{tm}(x, \{\theta_{tm,l}\}_{l=1\dots 4}), \quad (4)$$

where ϕ_{tm} is a 4-layer CNN with 32 channel dimension and the $\theta_{tm,l}$ weights for the l -th layer. In MBISPLD, the ϕ_{tm} consists of only 1×1 convolutions and statically optimized. This limited structure helps to stabilize training, but we extended it to cover more diverse mapping. The proposed DTM uses 3×3 dynamic convolutions [48, 6] whose kernels are dynamically determined by the DPS. In the DTM, the parameter dictionary $D_{\theta_{tm}}$ is learned for each $\theta_{tm,l}$. That is, $D_{\theta_1} = \{D_{\theta_{tm,l}}\}_{l=1\dots 4}$ and each $D_{\theta_{tm,l}}$ includes K candidate parameters for the l -th layer. The $\theta_{tm,l}$ is determined as follows:

$$\theta_{tm,l} = f_{DPS}(g_x, g_r, g_1, D_{\theta_{tm,l}}), \quad (5)$$

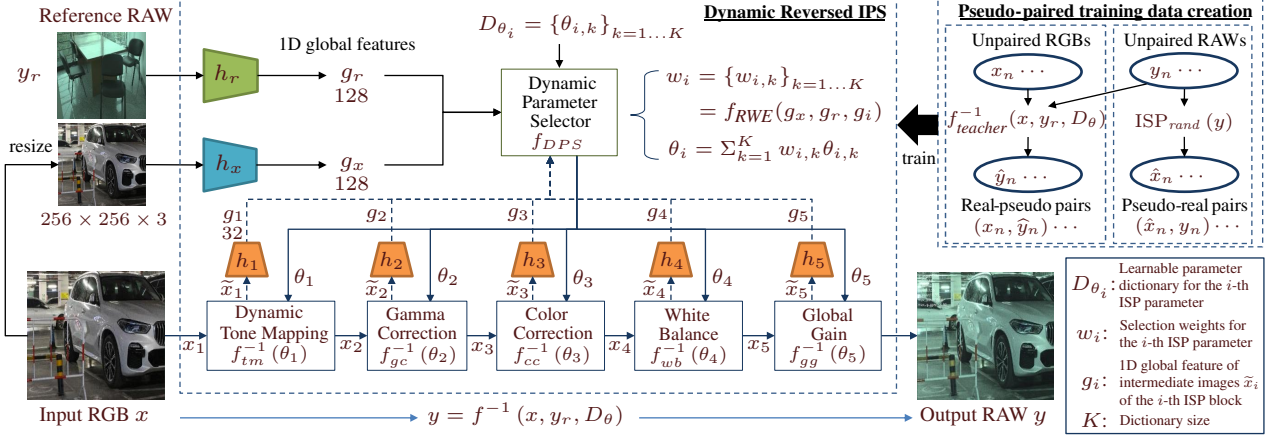


Figure 1. Our SRISP framework. An input RGB image and a reference RAW image are converted into 1D global features, and ISP parameters are dynamically determined based on them. To model complex mappings, a new reference-based dynamic CNN is incorporated as Dynamic Tone Mapping. Two types of pseudo-paired RGB and RAW images are used for stable training.

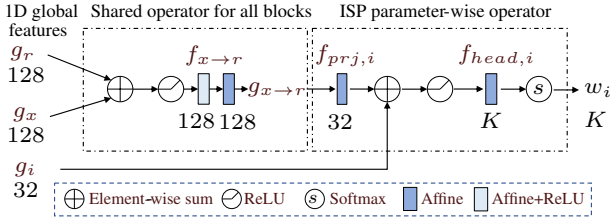


Figure 2. Reference-guided Weight Estimator f_{RWE} determines ISP parameter selection weights based on 1D global features calculated from an input image, a reference image, and intermediate features of the i -th ISP block.

where f_{DPS} expresses (2) and (3). The DTM has different parameter dictionaries for forward and reversed passes since this function is not invertible. Note that the original dynamic convolution selects its parameter based on input features of each convolution. On the other hand, our DTM determines the weights using global features of the input RGB and the reference RAW images.

3.3. Pseudo Pair Training

The proposed self-supervised learning using unpaired RGB and RAW images is realized by combining two types of pseudo RGB and RAW image pairs and our reference-guided DPS. The two types of pseudo-pairs are (1) PP_{rand} : the real-RAW y and pseudo-RGB \hat{x} pair generated by a random ISP and (2) PP_{MT} : the real-RGB x and pseudo-RAW \hat{y} pair generated by self-supervision based on Mean Teacher (MT) [45]. These pseudo-pairs do not represent the correspondence between real RGB and RAW images. Therefore, to learn fixed reversed pipeline using these pairs results in poor generalization for real RGB and RAW pairs. Moreover, MT converges to a meaningless solution when there is no correct label because MT basically just reduces noises of the labels. However, by combined with the reference-

guided DPS, these pseudo-pairs act as correct supervision. That is, in terms of dynamic parameter selection, our model is able to learn how to determine the mapping parameters for the given pair based on the reference, even if the pair is not a true pair. Furthermore, the learned parameter selection works with an unknown true RGB and RAW image pair.

The first pseudo pair, PP_{rand} , is defined as:

$$(\hat{x}, y) = (\text{ISP}_{rand}(y), y), \quad (6)$$

where ISP_{rand} is a simple forward ISP pipeline same as UPI [3]. Unlike UPI, the parameters of GG, CC, and GM are randomly determined independent of the target mapping, and a simple Gray-world algorithm [11] is used as WB. The implementation details are in the supplementary material. Although ISP_{rand} is different from real camera ISP, it is able to produce perceptually acceptable RGB images. By learning to reproduce the real RAW image y from this pseudo-RGB image \hat{x} as show in Figure 3, the proposed method learns the basic procedure of the RGB-to-RAW mapping. Unfortunately, RGB images generated by ISP_{rand} do not cover true diverse distribution of RGB images and it may degrade RAW reconstruction quality when the input is real RGB image. Therefore, the second pseudo-pair is needed.

The second pseudo-pair, PP_{MT} , is defined as:

$$(x, \hat{y}) = (x, f_{teacher}^{-1}(x, y_r, D_{\theta_{teacher}})), \quad (7)$$

where $f_{teacher}^{-1}$ and $D_{\theta_{teacher}}$ are MTs of f^{-1} and D_{θ} , respectively. We input a real RGB image x and reference real RAW image y_r randomly sampled from the RAW dataset into the MT and obtain an output RAW-like image \hat{y} . Note that x and y_r are unpaired. Figure 4 shows how to train the model using this pseudo pair. The key point here is to give \hat{y} as the reference y_r to the student model. This enables

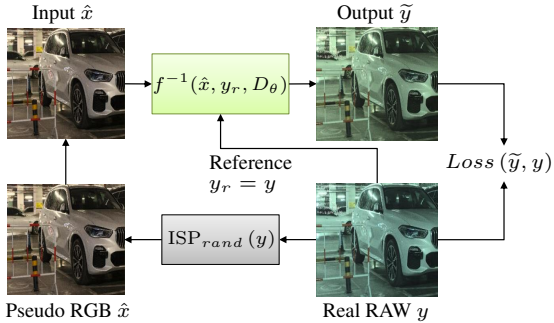


Figure 3. Randomized traditional ISP for creating the real RAW and pseudo RGB pair for training.

the student model to learn the RGB-to-RAW mapping without any contradiction even when the MT produces unnatural pseudo RAW images. On the other hand, if the real RAW image y set to y_r and \hat{y} is used only for student loss calculation as in the standard MT, the mismatch between y_r and the target \hat{y} leads to a wrong mapping. Note that this self-supervised learning is necessary to be combined with the PP_{rand} because the MT itself does not have a power to get close to the true mapping. The PP_{rand} enables the model to learn how to perform basic conversions to true RAW images, and the PP_{MT} enables the model to learn conversions from a variety of true RGB images. By combining these two with the reference-guided DPS, the proposed method achieves the un-paired learning.

3.4. Losses

Our goal is to build reversed ISP pipeline f^{-1} with its forward pipeline f is also trained as a constraint. Hence, the following bi-directional loss function is used:

$$L_{bi}(x, y) = |f_{gc}(y) - f_{gc}(f^{-1}(x))| + |x - f(y)|, \quad (8)$$

where f_{gc} is a gamma transformation with $\gamma = 2.2^{-1}$ introduced to encourage learning of dark areas as well as bright area. A similar idea was employed in [53]. We first process f^{-1} , and the same weights for the parameter selection are used for f . The final loss is a weighted sum of the losses for the first and second pseudo-pairs:

$$L = L_{bi}(\hat{x}, y) + \alpha L_{bi}(x, \hat{y}), \quad (9)$$

where α is a weight parameter and is set to 0.3 in this paper. The second term is not used in the first 15 epochs because outputs of the MT are not very meaningful.

4. Experiments

4.1. Datasets

We evaluated our method on three RAW image datasets and two RGB image datasets widely used in various re-

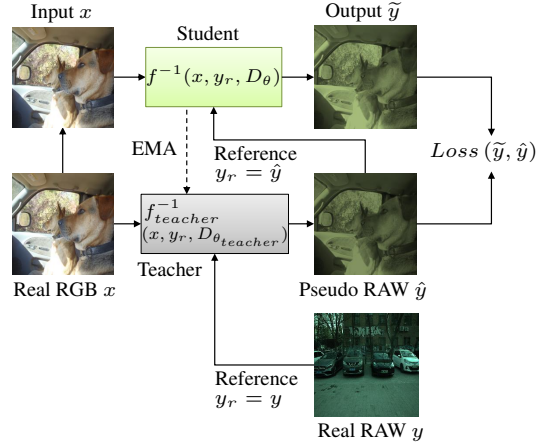


Figure 4. Mean Teacher model for creating the real RGB and pseudo RAW pair for training.

search including high-level computer vision studies. **MIT-Adobe-FiveK Dataset** [5]. We used the same train and test set used in [47] for Canon EOS 5D (777 images) and Nikon D700 (590 images). The LibRaw library was used to render RGB images from RAW images. **SIDD** [1]. This dataset provides 320 RGB and RAW image pairs captured by five smartphone cameras under different lighting conditions for training and 1280 patches for validation. **LOD Dataset** [15]. LOD Dataset contains low-light and normal-light RAW image pairs of eight object categories. We used normal-light images with 1830 training and 400 test images. We converted the original images to the DNG format by the Adobe DNG Converter and used full-size thumbnail images as RGB images. **COCO Dataset** [29]. Large-scale real world object images in RGB format are provided. We used 2017 Train images (118K images) for the PP_{MT} training and 2017 Val images (5K) for unpaired evaluation. **Flickr 1 Million Dataset** [35]. This dataset also provides diverse real world RGB images. We randomly sampled 200K images for the PP_{MT} training and 5K images for unpaired evaluation from 1M images.

4.2. Implementation Details

We used the following settings for all experiments. The image encoder h_r and h_x were 5-layer CNNs with 3×3 convolutions of stride 2 followed by ReLU activation except for the last layer. The channel sizes were $\{32, 64, 128, 128, 128\}$. The h_i had slightly different structure, i.e., 4-layer CNN with $\{32, 32, 32, 32\}$ channel size. The global average pooling was applied to the outputs of h_r , h_x , and h_i . The parameter dictionary size K was 5. The length of global feature vector g_r , g_x , $g_{x \rightarrow r}$ and g_i were 128, 128, 128, and 32, respectively. The network was trained for 800 epochs from scratch using Adam optimizer [23]. The initial learning rate was 10^{-4} with decay of 0.1 after 250 and 500 epochs. The mini-batch size was 24. As for our method,

Train	Method	Nikon D700		Canon EOS 5D		SIDD		LOD	
		AE↓	PSNR↑	AE↓	PSNR↑	AE↓	PSNR↑	AE↓	PSNR↑
	UPI [3]	7.80	27.93	7.35	32.97	8.82	36.29	8.40	30.69
	CycleISP [53]	8.80	30.51	9.80	32.14	9.49	42.07	10.35	22.33
Real	U-Net [8]	4.83	38.01	4.73	41.53	7.76	45.44	6.06	38.94
	MBISPLD [7]	4.72	38.49	4.72	41.38	7.60	45.56	6.22	37.74
	Ours w/o PP _{MT}	2.53	43.05	2.84	45.92	4.77	49.20	4.62	40.20
	Ours (Flickr)	2.56	43.13	2.93	45.54	4.92	48.72	4.64	40.20
	Ours (COCO)	2.57	43.32	2.90	45.64	4.96	48.85	4.64	39.66
Pseudo	Ours w/o PP _{MT}	4.55	34.67	4.00	37.89	6.86	42.79	5.05	35.17
	Ours (Flickr)	3.81	35.51	3.72	37.97	5.84	43.68	4.91	34.64
	Ours (COCO)	3.61	35.52	3.59	38.36	6.00	43.51	4.90	34.96
	Ours (All)	3.02	38.80	3.20	41.18	5.23	46.23	4.91	34.89

Table 1. Quantitative RAW reconstruction results among our methods and other methods. The characters in parentheses of ours denotes the dataset used for the PP_{MT}. “Real” and “Pseudo” indicate whether the real paired data or the PP_{rand} was used for training.

16 images were the first pseudo pairs and 8 images were the second pseudo pairs. The EMA decay of MT was 0.999. We used whole images for training rather than cropped patches [47]. In the training, the input images were resized into 256×256 , and random flip and rotation were applied. All RAW images were normalized into $[0, 1]$ using the black-level and white-level and applied the bilinear demosaicing for both training and evaluation.

4.3. Results

We compared our method against several state-of-the-art methods: **UPI** [3], a model based invertible ISP. We used the official parameters determined by metadata of Darmstadt Noise Dataset [41]. **CycleISP** [53], a DNN-based reversed ISP method. We utilized their pre-trained rgb2raw joint model trained with MIT-Adobe-FiveK Dataset and SIDD. The final mosaicing function was removed for our evaluation. **U-Net** [8], a simple U-Net [43] based method used in [8] as a baseline. We removed the final interpolation layer for mosaicing. **MBISPLD** [7], a hybrid method of the model-based and learning-based approach. We implemented this method by ourselves because there was no public code at that time. Our implemented MBISPLD consisted of unified Gain&WB, CC, GM with a single parameter, and TM with static 1×1 convolutions. Note that we did not use the Mosaicing and Lens-shading blocks as with our method. As for U-Net and MBISPLD, we trained them from scratch for each dataset using real RGB and RAW pairs with the same training settings of our method.

We also evaluated several variations of our method. We trained our model with the real image pairs same as U-Net and MBISPLD instead of the PP_{rand}. We denote it as “Real” and the original setting as “Pseudo” training. “Ours w/o PP_{MT}” is the model trained without the PP_{MT}. “Ours (Flickr/COCO)” is the model trained with the PP_{MT} generated from each RAW dataset and Flickr or COCO. “Ours (All)” is the model trained with all RAW and RGB datasets.

4.3.1 RAW Image Reconstruction

It is difficult to evaluate how well the input RGB image is mapped to the RAW image similar to the reference RAW image quantitatively because the perfect ground truth cannot be created in principle. Hence, in this evaluation, we divided each RAW and RGB image in half, and used the left RAW image as a reference y_{ref} , the right RGB image as an input x , and the right RAW image as a ground truth y with the assumption that the left and right region has the same characteristics of the sensing device and lighting. Table 1 shows reconstruction results on each dataset in terms of PSNR [dB] and the mean Angular Error (AE) [°] [16] between the predicted color and the true color. All our method achieved lower AE, which indicates more accurate reproduction of the global illumination, than the other methods. It is also shown that our proposed PP_{MT} (Flickr/COCO/All) reduced AE when only pseudo image pairs (Pseudo) were used. This is because the influence of the difference between the pseudo RGB images generated by ISP_{rand} and real RGB images was reduced by PP_{MT}. Furthermore, it is surprising that ours (All) achieved the comparable PSNR and lower AE compared to the other methods learned with the real pairs. We consider our method benefited from the data volume of multiple datasets thanks to the flexible pipeline based on the proposed DPS. In the setting using the real image pairs (Real), our methods further outperformed the other methods. It was hard for the other methods to solve the one-to-many mapping. On the other hand, ours was able to solve it by reformulating it as one-to-one mapping using the reference image.

4.3.2 Robustness to Unknown ISPs & Sensors

Table 2 shows the results of evaluating each method learned in Table 1 against MIT-Adobe FiveK dataset. We chose RGB images generated by unknown ISPs manually tuned by expert C per image as input RGB images. The proposed

Train	Method	Nikon Expert C		Canon Expert C	
		AE↓	PSNR↑	AE↓	PSNR↑
	UPI [3]	10.73	26.31	11.01	27.12
	CycleISP [53]	11.01	21.73	11.31	22.11
Real	U-Net [8]	8.28	19.81	9.08	20.35
	MBISPLD [7]	7.61	19.36	8.64	20.26
	Ours w/o PP _{MT}	9.62	23.47	7.15	28.65
Pseudo	Ours w/o PP _{MT}	6.22	31.20	5.39	33.35
	Ours (Flickr)	5.43	32.12	5.06	33.61
	Ours (COCO)	5.36	31.77	4.99	33.22
	Ours (All)	4.68	31.53	4.53	33.67

Table 2. Quantitative RAW reconstruction results on the images processed by the unknown ISP tuned by an expert [5].

Train	Method	Test PSNR↑			
		Nikon	Canon	SIDD	LOD
Nikon	R U-Net	38.01	39.62	33.84	19.00
	R MBISPLD	38.38	39.18	33.60	18.63
	P Ours (Flickr)	35.51	37.77	42.81	34.11
Canon	R U-Net	36.93	41.53	35.02	19.52
	R MBISPLD	37.39	41.35	34.77	19.27
	P Ours (Flickr)	35.35	37.97	43.19	34.43
SIDD	R U-Net	29.98	32.16	45.44	21.46
	R MBISPLD	30.74	32.85	45.56	21.05
	P Ours (Flickr)	34.70	37.49	43.68	32.37
LOD	R U-Net	24.08	26.05	35.32	38.94
	R MBISPLD	24.13	26.16	35.22	37.73
	P Ours (Flickr)	37.69	40.18	44.99	34.64

Table 3. Cross dataset evaluation to test generalization to different cameras. ‘‘R’’ and ‘‘P’’ denote the real-pair and the PP_{rand} training, respectively.

method reconstructed them with higher accuracy than the other methods. The proposed models learned by the pseudo pairs were more accurate than those learned by the real pairs. This indicates that the training without the assumption of a single pipeline is a key to realize the generalized parameter control. For a similar evaluation, Table 3 shows the results of applying the model learned on each dataset to another dataset. Note that FiveK, SIDD, and LOD used different ISPs for rendering RGB images. Our method generalized well to arbitrary ISPs and sensors, although other methods were only accurate for the learned ISP.

4.3.3 Unpaired Evaluation

We evaluated whether each method was able to convert the actual RGB datasets (i.e., Flickr and COCO) to RAW-like datasets. Since there is no ground truth, we compared the distribution of pixel values between all reference and generated RAW images. Specifically, we used Lab Histogram Intersections (HI) that are used to compare the color marginal distributions of images in the Lab color space [18]. Table 4 reports the average histogram intersection over all channels of all pixels. The proposed method using the two types of pseudo pairs produced the closest distribution to the reference compared to the other methods. The score of ours

(All) was worse on SIDD compared to ours learned for each dataset. The SIDD differs from other datasets in that it has fewer images and contains significantly dark RAW images. Those samples are minor in the mixed dataset, and it might have caused the degradation of ours (All). However, ours (All) still achieved better reconstruction results compared to the other methods.

4.3.4 Ablation Studies

Table 5 shows the effectiveness of our proposed modules, i.e., DPS, GG, DTM, and PP_{MT}, evaluated on the Canon EOS 5D. Each module contributed to the performance. In particular, the effect of DPS was significant (-5.87°, +8.27dB), followed by DTM (-0.55°, +1.02dB) and GG (-0.04°, +1.14dB). The PP_{MT} mainly contributed to generalization to unknown ISPs. On the other hand, all metrics were degraded if we replaced PP_{MT} with PP_{MT}⁻ or SL. From the result, we concluded that the proposed PP_{MT} effectively realized learning on the unpaired data.

4.3.5 Quantitative Results

We show qualitative comparisons against the other methods in Figure 5. The first and the second row show the results for the normal Canon EOS 5D and the Expert C image, respectively. The small images on the results of our method are the given reference images. The proposed method produced RAW-like images that have less color or brightness misalignment than the other methods. Although MBISPLD learned with the real pairs of Canon EOS 5D, it failed to reproduce the ambient light color that is removed in the input RGB image. The Expert C image was manually adjusted to be bright, so the other methods resulted in producing brighter images than the real RAW image. On the other hand, our method produced more GT-like RAW image thanks to the reference guidance.

4.3.6 RAW Image Object Detection

We used the LOD RAW-like images converted from the COCO’s RGB images by each method to learn 8 class object detection on the LOD dataset. Following [15], CenterNet [55] model pre-trained with COCO’s RGB images was fine-tuned using the LOD RAW-like images. The details are in the supplementary material. Table 6 shows the detection accuracy (mAP) of the trained model on the real LOD RAW images for normal-light condition. MBISPLD with the dictionary augmentation [7] (+DA) was also evaluated. Ours achieved the greatest accuracy improvement although all methods improved the pre-trained model. Our method successfully generated pseudo-RAW images effective for training in the down-stream task without the paired RGB and RAW images or metadata.

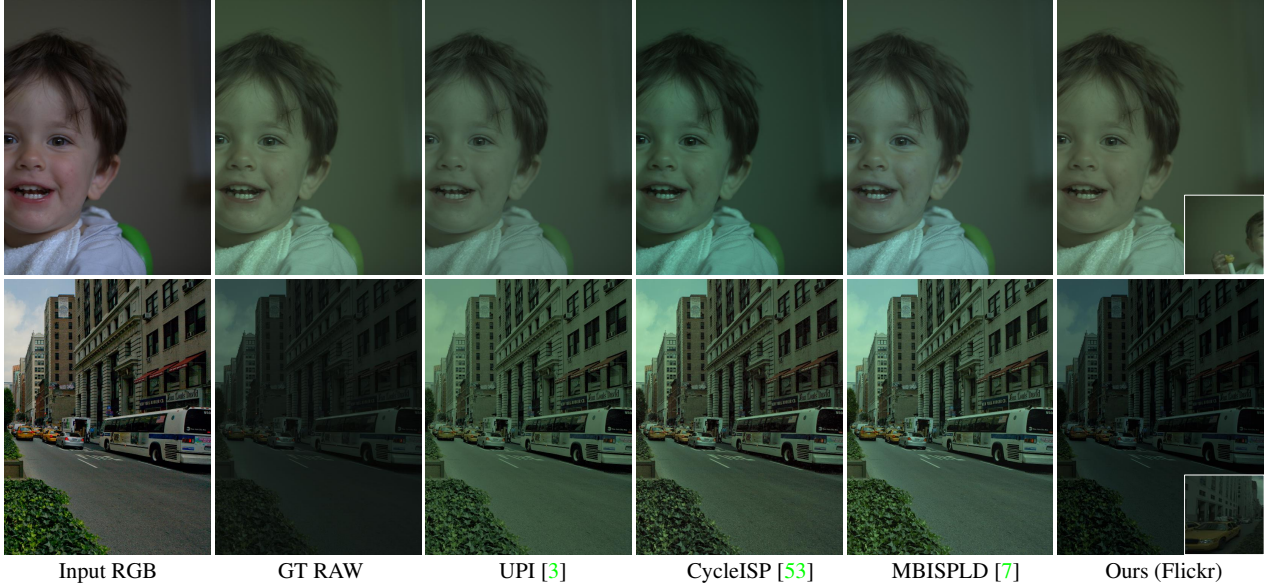


Figure 5. Qualitative RAW reconstruction results for Canon EOS 5D. The input RGB in the first row was processed by Libraw, and that in the second row was processed by the unknown ISP (expert tuning). The small images on ours are the reference images.

Train	Method	Flickr Histogram Intersection \uparrow				COCO Histogram Intersection \uparrow			
		Nikon	Canon	SIDD	LOD	Nikon	Canon	SIDD	LOD
Real	UPI [3]	0.731	0.761	0.707	0.662	0.692	0.732	0.659	0.640
	CycleISP [53]	0.408	0.389	0.511	0.398	0.407	0.390	0.518	0.401
	U-Net [8]	0.791	0.770	0.719	0.903	0.772	0.755	0.685	0.903
	MBISPLD [7]	0.795	0.768	0.731	0.883	0.785	0.765	0.715	0.896
Pseudo	Ours w/o PP_{MT}	0.715	0.822	0.688	0.899	0.686	0.817	0.651	0.899
	Ours (Flickr/COCO)	0.851	0.895	0.762	0.965	0.877	0.921	0.799	0.967
	Ours (All)	0.937	0.945	0.816	0.949	0.935	0.946	0.812	0.952

Table 4. Histogram Intersection (HI) in Lab color space between the generated RAW images and the reference RAW images.

Module				Canon EOS 5D		Flickr
DPS	GG	DTM	UT	AE \downarrow	PSNR \uparrow	HI \uparrow
				10.46	27.47	0.815
✓				4.59	35.74	0.898
✓	✓			4.55	36.87	0.901
✓	✓	✓		4.00	37.89	0.900
✓	✓	✓	SL	4.17	37.16	0.908
✓	✓	✓	PP_{MT}^-	4.97	35.64	0.907
✓	✓	✓	PP_{MT}	3.72	37.97	0.940

Table 5. Ablation studies of the proposed modules. UT denotes Unpaired Training. PP_{MT} is the proposed second pseudo-pair training, and PP_{MT}^- is the version that uses the target RAW image as the reference image for the student. SL is Style Loss [19]

5. Conclusion

In this paper, we have proposed a self-supervised reversed ISP method that does not require metadata and paired images. The proposed method is able to handle

Fine-tuning data	mAP@0.5:0.95
No fine-tuning	41.60
UPI [8]	46.03
MBISPLD [7]	46.37
MBISPLD+DA [7]	46.47
Ours (COCO)	47.17

Table 6. Object detection accuracy on LOD Dataset with fine-tuning using RAW-like data converted from COCO Dataset

diverse RGB-to-RAW mappings by learning how to control the mapping parameters based on a given reference RAW image. Furthermore, the entire pipeline is trainable using unpaired RGB and RAW images. The experiments showed the proposed method successfully produced the target RAW-like images. We hope this approach will contribute to the future progress of the RAW image-based computer vision research.

References

- [1] Abdelrahman Abdelhamed, Stephen Lin, and Michael S. Brown. A high-quality denoising dataset for smartphone cameras. In *2018 IEEE/CVF Conference on Computer Vision and Pattern Recognition*, pages 1692–1700, 2018. [1](#), [4.1](#)
- [2] Mahmoud Afifi, Abdelrahman Abdelhamed, Abdullah Abuolaim, Abhijith Punnappurath, and Michael S Brown. Cie xyz net: Unprocessing images for low-level computer vision tasks. *IEEE Transactions on Pattern Analysis and Machine Intelligence*, 44(9):4688–4700, 2021. [1](#), [2.1](#)
- [3] Tim Brooks, Ben Mildenhall, Tianfan Xue, Jiawen Chen, Dillon Sharlet, and Jonathan T Barron. Unprocessing images for learned raw denoising. In *Proceedings of the IEEE/CVF Conference on Computer Vision and Pattern Recognition*, pages 11036–11045, 2019. [1](#), [3](#), [3.3](#), [4.1](#), [4.3](#), [4.3.2](#), [4.3.3](#), [4.3.3](#), [A.1.1](#), [A.1.3](#), [A.2](#)
- [4] Mark Buckler, Suren Jayasuriya, and Adrian Sampson. Reconfiguring the imaging pipeline for computer vision. In *Proceedings of the IEEE International Conference on Computer Vision*, pages 975–984, 2017. [2.2](#)
- [5] Vladimir Bychkovsky, Sylvain Paris, Eric Chan, and Frédo Durand. Learning photographic global tonal adjustment with a database of input / output image pairs. In *The Twenty-Fourth IEEE Conference on Computer Vision and Pattern Recognition*, 2011. [1](#), [4.1](#), [2](#), [A.2](#)
- [6] Yinpeng Chen, Xiyang Dai, Mengchen Liu, Dongdong Chen, Lu Yuan, and Zicheng Liu. Dynamic convolution: Attention over convolution kernels. In *Proceedings of the IEEE/CVF Conference on Computer Vision and Pattern Recognition*, pages 11030–11039, 2020. [3.2](#)
- [7] Marcos V Conde, Steven McDonagh, Matteo Maggioni, Ales Leonardis, and Eduardo Pérez-Pellitero. Model-based image signal processors via learnable dictionaries. In *Proceedings of the AAAI Conference on Artificial Intelligence*, volume 36, pages 481–489, 2022. [1](#), [2.1](#), [3](#), [4.1](#), [4.3](#), [4.3.2](#), [4.3.3](#), [4.3.3](#), [A.1.1](#), [A.1.3](#), [A.3](#), [A.3](#), [B.1](#)
- [8] Marcos V Conde, Radu Timofte, et al. Reversed Image Signal Processing and RAW Reconstruction. AIM 2022 Challenge Report. In *Proceedings of the European Conference on Computer Vision Workshops (ECCVW)*, 2022. [1](#), [2.1](#), [4.1](#), [4.3](#), [4.3.2](#), [4.3.3](#), [4.3.6](#), [A.3](#), [B.1](#)
- [9] Ziteng Cui, Kunchang Li, Lin Gu, Shenghan Su, Peng Gao, ZhengKai Jiang, Yu Qiao, and Tatsuya Harada. You only need 90k parameters to adapt light: a light weight transformer for image enhancement and exposure correction. In *33rd British Machine Vision Conference 2022, BMVC 2022, London, UK, November 21-24, 2022*. BMVA Press, 2022. [2.2](#)
- [10] Xiaoyi Dong, Yu Zhu, Chenghua Li, Peisong Wang, and Jian Cheng. Rispnet: a network for reversed image signal processing. In *Computer Vision–ECCV 2022 Workshops: Tel Aviv, Israel, October 23–27, 2022, Proceedings, Part II*, pages 445–457. Springer, 2023. [2.1](#)
- [11] Marc Ebner. *Color constancy*, volume 7. John Wiley & Sons, 2007. [3.3](#), [A.2](#)
- [12] Nikolaus Hansen and Andreas Ostermeier. Adapting arbitrary normal mutation distributions in evolution strategies: The covariance matrix adaptation. In *Proceedings of IEEE international conference on evolutionary computation*, pages 312–317. IEEE, 1996. [2.2](#)
- [13] Luis V Hevia, Miguel A Patricio, José M Molina, and Antonio Berlanga. Optimization of the isp parameters of a camera through differential evolution. *IEEE Access*, 8:143479–143493, 2020. [1](#), [2.2](#)
- [14] Jonathan Ho, Xi Chen, Aravind Srinivas, Yan Duan, and Pieter Abbeel. Flow++: Improving flow-based generative models with variational dequantization and architecture design. In *International Conference on Machine Learning*, pages 2722–2730. PMLR, 2019. [2.1](#)
- [15] Yang Hong, Kaixuan Wei, Linwei Chen, and Ying Fu. Crafting object detection in very low light. In *Proceedings of the British Machine Vision Virtual Conference*, 2021. [1](#), [4.1](#), [4.3.6](#), [A.4](#)
- [16] Steven D Hordley and Graham D Finlayson. Re-evaluating colour constancy algorithms. In *Proceedings of the 17th International Conference on Pattern Recognition, ICPR 2004.*, volume 1, pages 76–79. IEEE, 2004. [4.3.1](#)
- [17] Andrey Ignatov, Luc Van Gool, and Radu Timofte. Replacing mobile camera isp with a single deep learning model. In *Proceedings of the IEEE/CVF Conference on Computer Vision and Pattern Recognition Workshops*, pages 536–537, 2020. [1](#)
- [18] Phillip Isola, Jun-Yan Zhu, Tinghui Zhou, and Alexei A Efros. Image-to-image translation with conditional adversarial networks. In *Proceedings of the IEEE conference on computer vision and pattern recognition*, pages 1125–1134, 2017. [4.3.3](#)
- [19] Justin Johnson, Alexandre Alahi, and Li Fei-Fei. Perceptual losses for real-time style transfer and super-resolution. In *Computer Vision–ECCV 2016: 14th European Conference, Amsterdam, The Netherlands, October 11–14, 2016, Proceedings, Part II 14*, pages 694–711. Springer, 2016. [5](#)
- [20] Hakki Can Karaimer and Michael S Brown. A software platform for manipulating the camera imaging pipeline. In *Computer Vision–ECCV 2016: 14th European Conference, Amsterdam, The Netherlands, October 11–14, 2016, Proceedings, Part I 14*, pages 429–444. Springer, 2016. [1](#)
- [21] Jinha Kim, Jun Jiang, and Jinwei Gu. Overexposure mask fusion: Generalizable reverse isp multi-step refinement. In *Computer Vision–ECCV 2022 Workshops: Tel Aviv, Israel, October 23–27, 2022, Proceedings, Part II*, pages 699–713. Springer, 2023. [2.1](#)
- [22] Seon Joo Kim, Hai Ting Lin, Zheng Lu, Sabine Süsstrunk, Stephen Lin, and Michael S Brown. A new in-camera imaging model for color computer vision and its application. *IEEE Transactions on Pattern Analysis and Machine Intelligence*, 34(12):2289–2302, 2012. [1](#)
- [23] Diederik P Kingma and Jimmy Ba. Adam: A method for stochastic optimization. *arXiv preprint arXiv:1412.6980*, 2014. [4.2](#), [A.4](#)
- [24] Durk P Kingma and Prafulla Dhariwal. Glow: Generative flow with invertible 1x1 convolutions. *Advances in neural information processing systems*, 31, 2018. [2.1](#)

- [25] Furkan Kınlı, Barış Özcan, and Furkan Kırac. Reversing image signal processors by reverse style transferring. In *Computer Vision—ECCV 2022 Workshops: Tel Aviv, Israel, October 23–27, 2022, Proceedings, Part II*, pages 688–698. Springer, 2023. [2.1](#)
- [26] Chen Li and Gim Hee Lee. From synthetic to real: Unsupervised domain adaptation for animal pose estimation. In *Proceedings of the IEEE/CVF conference on computer vision and pattern recognition*, pages 1482–1491, 2021. [2.3](#)
- [27] Yu-Jhe Li, Xiaoliang Dai, Chih-Yao Ma, Yen-Cheng Liu, Kan Chen, Bichen Wu, Zijian He, Kris Kitani, and Peter Vajda. Cross-domain adaptive teacher for object detection. In *IEEE Conference on Computer Vision and Pattern Recognition*, 2022. [2.3](#)
- [28] Chih-Hung Liang, Yu-An Chen, Yueh-Cheng Liu, and Winston H Hsu. Raw image deblurring. *IEEE Transactions on Multimedia*, 24:61–72, 2020. [1](#)
- [29] Tsung-Yi Lin, Michael Maire, Serge Belongie, James Hays, Pietro Perona, Deva Ramanan, Piotr Dollár, and C Lawrence Zitnick. Microsoft coco: Common objects in context. In *European conference on computer vision*, pages 740–755. Springer, 2014. [1](#), [4.1](#), [A.2](#), [A.4](#)
- [30] Hanxiao Liu, Karen Simonyan, and Yiming Yang. Darts: Differentiable architecture search. *arXiv preprint arXiv:1806.09055*, 2018. [2.2](#)
- [31] Shuai Liu, Chaoyu Feng, Xiaotao Wang, Hao Wang, Ran Zhu, Yongqiang Li, and Lei Lei. Deep-flexisp: A three-stage framework for night photography rendering. In *Proceedings of the IEEE/CVF Conference on Computer Vision and Pattern Recognition*, pages 1211–1220, 2022. [1](#)
- [32] Yen-Cheng Liu, Chih-Yao Ma, Zijian He, Chia-Wen Kuo, Kan Chen, Peizhao Zhang, Bichen Wu, Zsolt Kira, and Peter Vajda. Unbiased teacher for semi-supervised object detection. In *Proceedings of the International Conference on Learning Representations*, 2021. [2.3](#)
- [33] Yen-Cheng Liu, Chih-Yao Ma, and Zsolt Kira. Unbiased teacher v2: Semi-supervised object detection for anchor-free and anchor-based detectors. In *Proceedings of the IEEE/CVF Conference on Computer Vision and Pattern Recognition*, pages 9819–9828, June 2022. [2.3](#)
- [34] Ilya Loshchilov and Frank Hutter. Sgdr: Stochastic gradient descent with warm restarts. *arXiv preprint arXiv:1608.03983*, 2016. [A.4](#)
- [35] B. Thomee Mark J. Huiskes and Michael S. Lew. New trends and ideas in visual concept detection: The mir flickr retrieval evaluation initiative. In *MIR '10: Proceedings of the 2010 ACM International Conference on Multimedia Information Retrieval*, pages 527–536, New York, NY, USA, 2010. ACM. [1](#), [4.1](#), [A.2](#)
- [36] Igor Morawski, Yu-An Chen, Yu-Sheng Lin, Shushil Dangi, Kai He, and Winston H Hsu. Genisp: Neural isp for low-light machine cognition. In *Proceedings of the IEEE/CVF Conference on Computer Vision and Pattern Recognition*, pages 630–639, 2022. [1](#), [2.2](#)
- [37] Ali Mosleh, Avinash Sharma, Emmanuel Onzon, Fahim Mannan, Nicolas Robidoux, and Felix Heide. Hardware-in-the-loop end-to-end optimization of camera image processing pipelines. In *Proceedings of the IEEE/CVF Conference on Computer Vision and Pattern Recognition*, pages 7529–7538, 2020. [1](#), [2.2](#)
- [38] Jun Nishimura, Timo Gerasimow, Rao Sushma, Aleksandar Sutic, Chyuan-Tyng Wu, and Gilad Michael. Automatic isp image quality tuning using nonlinear optimization. In *2018 25th IEEE International Conference on Image Processing (ICIP)*, pages 2471–2475. IEEE, 2018. [1](#), [2.2](#)
- [39] Emmanuel Onzon, Fahim Mannan, and Felix Heide. Neural auto-exposure for high-dynamic range object detection. In *Proceedings of the IEEE/CVF Conference on Computer Vision and Pattern Recognition*, pages 7710–7720, 2021. [2.2](#)
- [40] G Pavithra and Bhat Radhesh. Automatic image quality tuning framework for optimization of isp parameters based on multi-stage optimization approach. *Electronic Imaging*, 2021(9):197–1, 2021. [1](#), [2.2](#)
- [41] Tobias Plotz and Stefan Roth. Benchmarking denoising algorithms with real photographs. In *Proceedings of the IEEE conference on computer vision and pattern recognition*, pages 1586–1595, 2017. [4.3](#), [A.2](#)
- [42] Nicolas Robidoux, Luis E Garcia Capel, Dong-eun Seo, Avinash Sharma, Federico Ariza, and Felix Heide. End-to-end high dynamic range camera pipeline optimization. In *Proceedings of the IEEE/CVF Conference on Computer Vision and Pattern Recognition*, pages 6297–6307, 2021. [1](#), [2.2](#)
- [43] Olaf Ronneberger, Philipp Fischer, and Thomas Brox. U-net: Convolutional networks for biomedical image segmentation. In *Medical Image Computing and Computer-Assisted Intervention—MICCAI 2015: 18th International Conference, Munich, Germany, October 5–9, 2015, Proceedings, Part III 18*, pages 234–241. Springer, 2015. [4.3](#)
- [44] Eli Schwartz, Raja Giryes, and Alex M Bronstein. Deepisp: Toward learning an end-to-end image processing pipeline. *IEEE Transactions on Image Processing*, 28(2):912–923, 2018. [1](#)
- [45] Antti Tarvainen and Harri Valpola. Mean teachers are better role models: Weight-averaged consistency targets improve semi-supervised deep learning results. *Advances in neural information processing systems*, 30, 2017. [1](#), [2.3](#), [3.3](#)
- [46] Ethan Tseng, Felix Yu, Yuting Yang, Fahim Mannan, Karl ST Arnaud, Derek Nowrouzezahrai, Jean-François Lalonde, and Felix Heide. Hyperparameter optimization in black-box image processing using differentiable proxies. *ACM Trans. Graph.*, 38(4):27–1, 2019. [1](#), [2.2](#)
- [47] Yazhou Xing, Zian Qian, and Qifeng Chen. Invertible image signal processing. In *CVPR*, 2021. [1](#), [2.1](#), [4.1](#), [4.2](#), [A.3](#)
- [48] Brandon Yang, Gabriel Bender, Quoc V Le, and Jiquan Ngiam. Condconv: Conditionally parameterized convolutions for efficient inference. *Advances in Neural Information Processing Systems*, 32, 2019. [3.2](#)
- [49] Masakazu Yoshimura, Junji Otsuka, Atsushi Irie, and Takeshi Ohashi. Dynamicisp: Dynamically controlled image signal processor for image recognition. *arXiv preprint arXiv:2211.01146*, 2022. [1](#), [2.2](#)
- [50] Masakazu Yoshimura, Junji Otsuka, Atsushi Irie, and Takeshi Ohashi. Rawgmt: Noise-accounted raw augmentation enables recognition in a wide variety of environments. *arXiv preprint arXiv:2210.16046*, 2022. [1](#)

- [51] Fisher Yu, Dequan Wang, Evan Shelhamer, and Trevor Darrell. Deep layer aggregation. In *Proceedings of the IEEE conference on computer vision and pattern recognition*, pages 2403–2412, 2018. [A.4](#)
- [52] Ke Yu, Zexian Li, Yue Peng, Chen Change Loy, and Jinwei Gu. Reconfigisp: Reconfigurable camera image processing pipeline. In *Proceedings of the IEEE/CVF International Conference on Computer Vision*, pages 4248–4257, 2021. [1](#), [2.2](#)
- [53] Syed Waqas Zamir, Aditya Arora, Salman Khan, Munawar Hayat, Fahad Shahbaz Khan, Ming-Hsuan Yang, and Ling Shao. Cycleisp: Real image restoration via improved data synthesis. In *Proceedings of the IEEE/CVF Conference on Computer Vision and Pattern Recognition*, pages 2696–2705, 2020. [1](#), [2.1](#), [3.4](#), [4.1](#), [4.3](#), [4.3.2](#), [4.3.3](#), [4.3.3](#)
- [54] Xuaner Zhang, Qifeng Chen, Ren Ng, and Vladlen Koltun. Zoom to learn, learn to zoom. In *Proceedings of the IEEE Conference on Computer Vision and Pattern Recognition*, 2019. [1](#)
- [55] Xingyi Zhou, Dequan Wang, and Philipp Krähenbühl. Objects as points. *arXiv preprint arXiv:1904.07850*, 2019. [4.3.6](#), [A.4](#)
- [56] Beiji Zou and Yue Zhang. Learned reverse isp with soft supervision. In *Computer Vision—ECCV 2022 Workshops: Tel Aviv, Israel, October 23–27, 2022, Proceedings, Part II*, pages 489–506. Springer, 2023. [2.1](#)

Appendices

A. Implementation Details

A.1. ISP Blocks

The proposed reversed ISP pipeline consists of five ISP blocks: Global Gain (GG) f_{gg} , White Balance (WB) f_{wb} , Color Correction (CC) f_{cc} , Gamma Correction (GC) f_{gc} , and Tone Mapping (TM) f_{tm} . In this section, we describe the detailed implementation of the blocks except for TM.

A.1.1 Global Gain

The forward function f_{gg} simply multiplies single scalar g over all pixels to adjust global brightness:

$$f_{gg}(x, g) = gx. \quad (10)$$

In MBISPLD [7], GG is unified into WB with a single parameter dictionary. We designed them separately with independent dictionaries to enhance their representation capability. In addition, we used a highlight preservation technique [3].

A.1.2 White Balance

The white balancing is an operation to remove global illumination effect and achieve color constancy. The f_{wb} is expressed as matrix multiplication of a matrix style input image $X \in \mathbb{R}^{HW \times 3}$ and a 3×3 diagonal matrix composed of channel-wise gains $[g_r, g_g, g_b]$:

$$f_{wb}(x, [g_r, g_g, g_b]) = X \text{diag}([g_r, g_g, g_b]). \quad (11)$$

We initialized K candidates of g_r and g_b in the parameter dictionary using a uniform distribution $\mathcal{U}(1, 2)$ and set g_g as 1.0 based on the traditional ISP pipeline. The highlight preservation technique was used as well as GG.

A.1.3 Color Correction

The color correction connects the camera specific RAW color space to the common linear sRGB space. The f_{cc} is expressed as matrix multiplication of X and a 3×3 Color Correction Matrix (CCM) M_{ccm} such that:

$$f_{cc}(x, M_{ccm}) = XM_{ccm}. \quad (12)$$

To maintain realistic M_{ccm} features, we applied column-normalization [3, 7] to M_{ccm} at every inference.

A.1.4 Gamma Correction

Human perception is more sensitive to darker region than brighter region. To adjust images for human perception, simple gamma correction is widely used:

$$f_{gc}(x, \gamma) = \max(x, 10^{-8})^{1/\gamma}. \quad (13)$$

We initialized K candidates of γ in the parameter dictionary using a uniform distribution $\mathcal{U}(1.7, 2.7)$ whose center is 2.2, which is commonly chosen for traditional ISP.

A.2. Randomized ISP

Figure 6 shows the pipeline of the ISP_{rand} that generates the PP_{rand}. We essentially followed the implementation of UPI [3], but the parameters of WB, GG, CC, and GM were determined independently of the target pipeline. The WB gains were determined by a simple WB algorithm based on the Gray-world assumption [11] without using any metadata. Specifically, per-channel averages of pixel values were used to determine the gains as follows:

$$(g_r, g_g, g_b) = \left(\frac{G_{mean}}{R_{mean}}, 1, \frac{G_{mean}}{B_{mean}} \right), \quad (14)$$

where R_{mean} , G_{mean} , and B_{mean} are the average pixel values for R, G, and B channels, respectively. To remove outliers, we calculated the luma Y in YCbCr color space first and excluded pixels whose Y values were top and bottom 5% for the mean calculating. The CCM of CC was generated with random interpolation of CCMs of irrelevant cameras obtained from Darmstadt Noise Dataset [41] and MIT-Adobe-FiveK Dataset [5]. The global gain and gamma parameters were sampled from uniform distributions $\mathcal{U}(1, 2)$ and $\mathcal{U}(2.2, 3.2)$, respectively. These values were determined to make images brighter because the UPI pipeline tends to generate darker images than the images in COCO [29] or Flickr 1 Million Dataset [35]. Instead of generating pseudo-RGB images on the fly at training time, we generated one RGB image from each RAW image before training to speed up experiments. Figure 7 shows examples of images generated by the ISP_{rand} for the Nikon, Canon, SIDD, and LOD images. Note that we applied the gamma correction with $\gamma = 2.2$ to all RAW images only for visualization.

A.3. Evaluation Metrics

In the evaluation with ground-truth RAW images, PSNR [dB] and Angular Error (AE) [°] were evaluated with the half split images as we described. That is, we used the left RAW image as the reference and the right RGB and RAW images as the input and ground-truth images. When we split the image horizontally, all images were rotated so that the long side became the width. In addition, the right RGB and RAW images were further split in half vertically, and

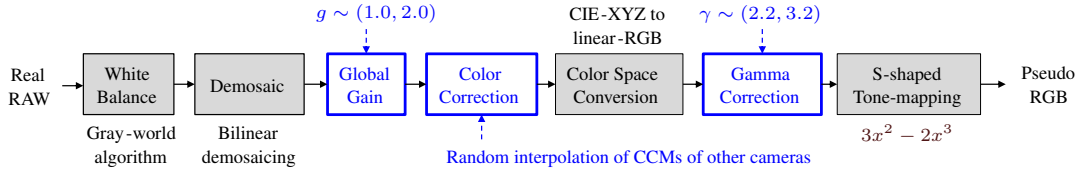


Figure 6. The pipeline of the randomized traditional ISP (ISP_{rand}) for the first pseudo pair (PP_{rand}) training.



Figure 7. Pseudo RGB images generated by the randomized traditional ISP (ISP_{rand}) for the first pseudo pair (PP_{rand}) training.

we evaluated them independently with the same reference image (the left image) to reduce GPU memory usage. This kind of split evaluation was also employed in [47, 7]. Note that other methods were also evaluated with the same split images.

In the evaluation without ground-truth RAW images, Histogram Intersention (HI) in Lab color space was used as an evaluation metric. To compute HI, first, each RAW pixel value was converted to CIE XYZ color space using the CCM of the reference RAW image. Second, the CIE XYZ values were converted to CIE Lab color space. Then, histograms of each channel in CIE Lab color space were calculated for all generated and reference RAW images. Finally, the averaged HI was calculated as follows:

$$HI = \frac{1}{3N} \sum_{c \in \{L, a, b\}} \sum_{j=1}^B \min(H_{ref,c}(j), H_{gen,c}(j)), \quad (15)$$

where $H_{ref,c}$ and $H_{gen,c}$ are the histograms with B bins for channel c of all reference and generated RAW images, N denotes the number of total pixels, and $H_{ref,c}(j)$

and $H_{gen,c}(j)$ are the number of pixels in the j -th bin. In this paper, we set B to 512 and the range of values to $[-150, 150]$. This metric indicates how close the two marginal distributions of pixels over all images are in terms of color and brightness.

All evaluation metrics reported in this paper are averaged values of three-time experiments with different random seeds.

A.4. RAW Image Object Detection

CenterNet [55] whose backbone is a modified DLA-34 [51] was used as a detector for eight class objects: car, motorbike, bicycle, chair, diningtable, bottle, tvmonitor, and bus [15]. The detector was initialized with COCO pre-trained model and trained for 40 epochs with Adam [23] optimizer using the pseudo COCO-RAW images generated by each reversed ISP method. A cosine decay learning rate schedule with a linear warmup [34] for the first 1,000 iterations whose maximum and minimum learning rates were 10^{-3} and 10^{-4} was used. The input size was (512, 512, 3), and random flip, random scaling, and random cropping

Data	Method	Nikon D700		Canon EOS 5D		SIDD		LOD	
		AE↓	PSNR↑	AE↓	PSNR↑	AE↓	PSNR↑	AE↓	PSNR↑
Pseudo	U-Net [8]	9.07	24.51	9.19	26.22	9.31	35.43	7.84	31.52
	U-Net (All) [8]	7.34	24.34	6.83	26.71	10.08	36.64	8.29	31.76
	MBISPLD [7]	7.35	23.66	7.32	25.63	8.53	36.95	8.84	34.10
	MBISPLD (All) [7]	9.70	23.37	8.62	25.39	10.81	36.01	7.96	34.50
	Ours (Flickr)	3.81	35.51	3.72	37.97	5.84	43.68	4.91	34.64
	Ours (COCO)	3.61	35.52	3.59	38.36	6.00	43.51	4.90	34.96
	Ours (All)	3.02	38.80	3.20	41.18	5.23	46.23	4.91	34.89

Table 7. Quantitative RAW reconstruction results among our methods and other methods trained without the real paired images. The characters (Flickr/COCO) in parentheses of ours denote the dataset used for the PP_{MT} . Ours (All) was trained with the PP_{rand} and PP_{MT} generated from all datasets. U-Net (All) and MBISPLD (All) were trained with PP_{rand} generated from all datasets.

were used as data augmentation. In addition, we also applied the RAW image noise injection proposed in [15] to the pseudo RAW images because the pseudo RAW images generated from COCO dataset [29] contain less noises than real RAW images of LOD dataset [15]. Any color jitter and contrast augmentation were not used. We evaluated the detectors’ performance with average precision (AP@0.5:0.95) [29] for real LOD-RAW test images of three-time experiments with different random seeds.

B. Additional Results

B.1. Training Other Methods without Real-pairs

To verify the importance of combining the proposed pseudo-pairs and model architecture, we trained U-Net [8] and MBISPLD [7] with the same PP_{rand} as ours and evaluated them. Table 7 shows RAW image reconstruction results of ours and the other methods trained without the real paired data on each dataset. Compared with the proposed method, the other methods were not effectively trained using the PP_{rand} , which requires assuming multiple ISP pipelines. This is because it was difficult to estimate the parameters of the forward ISP from the input RGB image alone. As a result, in the training using all data, only ours (all) was able to improve the accuracy greatly with the benefit of the data amount. It shows that the proposed reference-guided DPS plays an important role in the pseudo-pair training.

B.2. Qualitative Results for RAW Image Datasets

Figure 8, Figure 9, and Figure 10 show qualitative RAW reconstruction results for LOD dataset, Nikon D700 (expert C tuning), and Canon EOS 5D (expert C tuning), respectively. Thanks to the reference guidance, ours was able to generate more ground-truth-like images than the other methods which were trained with the real image pairs. Although U-Net and MBISPLD had the knowledge of the ISP pipeline of LOD dataset, they failed to reconstruct the illumination color because there was no clue in the input RGB image to estimate the color. However, our method also has

a issue in reconstructing highlight region. The bright area of the generated images by ours tends to be darker than that of the ground-truth RAW images. This issue may have been caused by the design of the loss function, which focuses on reconstructing dark areas. We suspect that the process of matching global brightness and color was more emphasized than restoring highlight areas since the pixels in a RAW image were essentially dark. The introduction of losses that encourage the restoration of highlights and maintain the high dynamic range is a future work.

B.3. Qualitative Results for RGB Image Datasets

Figure 11 and Figure 12 show RAW-like images converted from RGB images in Flickr or COCO dataset by our methods. RAW images were sampled from RAW image datasets (Nikon/Canon/SIDD/LOD) and given as reference images for the proposed method trained on each RAW and RGB dataset. The proposed method was able to generate multiple RAW-like images from one input RGB image by changing the reference images. These results show that our method enables us to obtain diverse RAW-like images with a combination of source RGB and target RAW images.

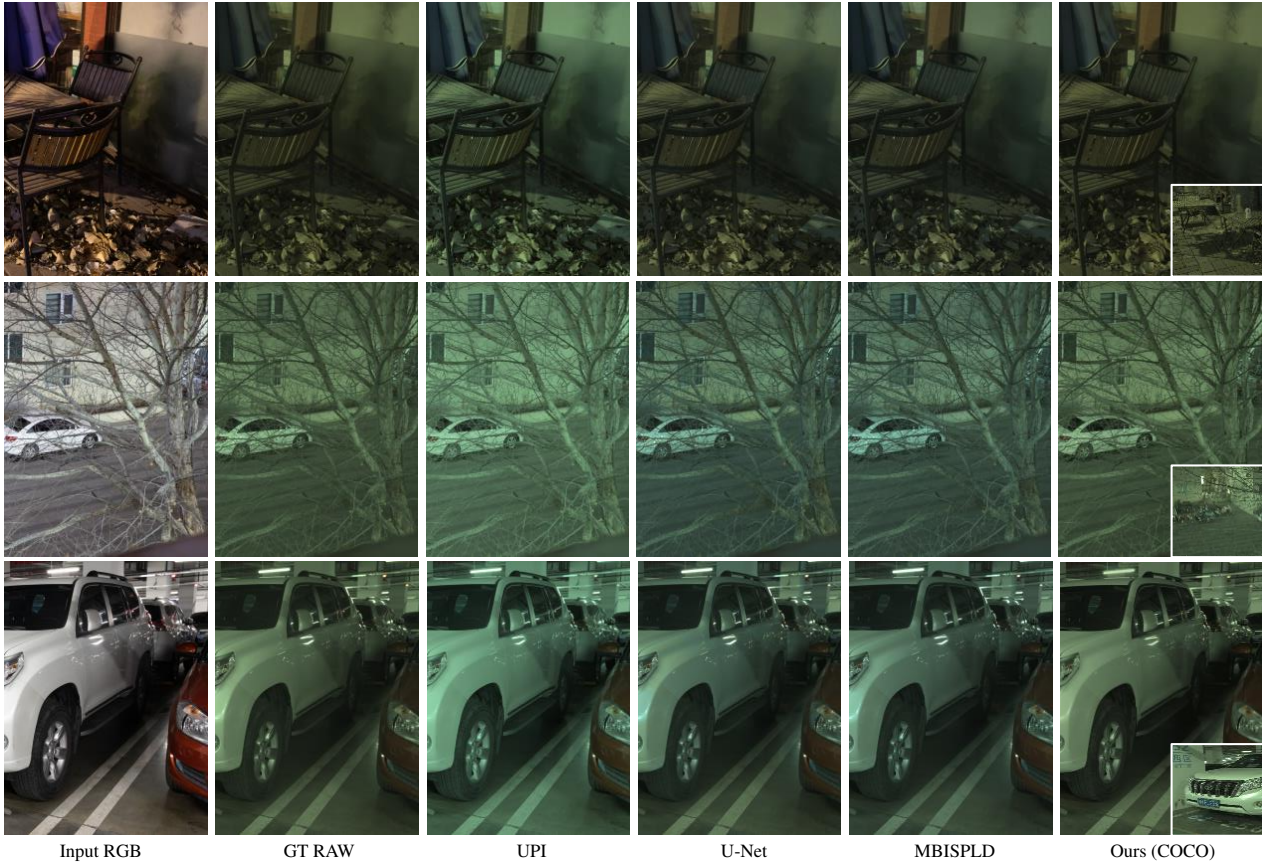


Figure 8. Qualitative RAW reconstruction results for LOD Dataset. U-Net and MBISPLD were trained with the real-pairs of LOD Dataset, and ours (COCO) was trained with only the proposed pseudo-pairs (PP_{rand} and PP_{MT} for LOD and COCO dataset). The small images on ours are the reference images. The gamma correction with $\gamma = 2.2$ was applied to all RAW images only for visualization.

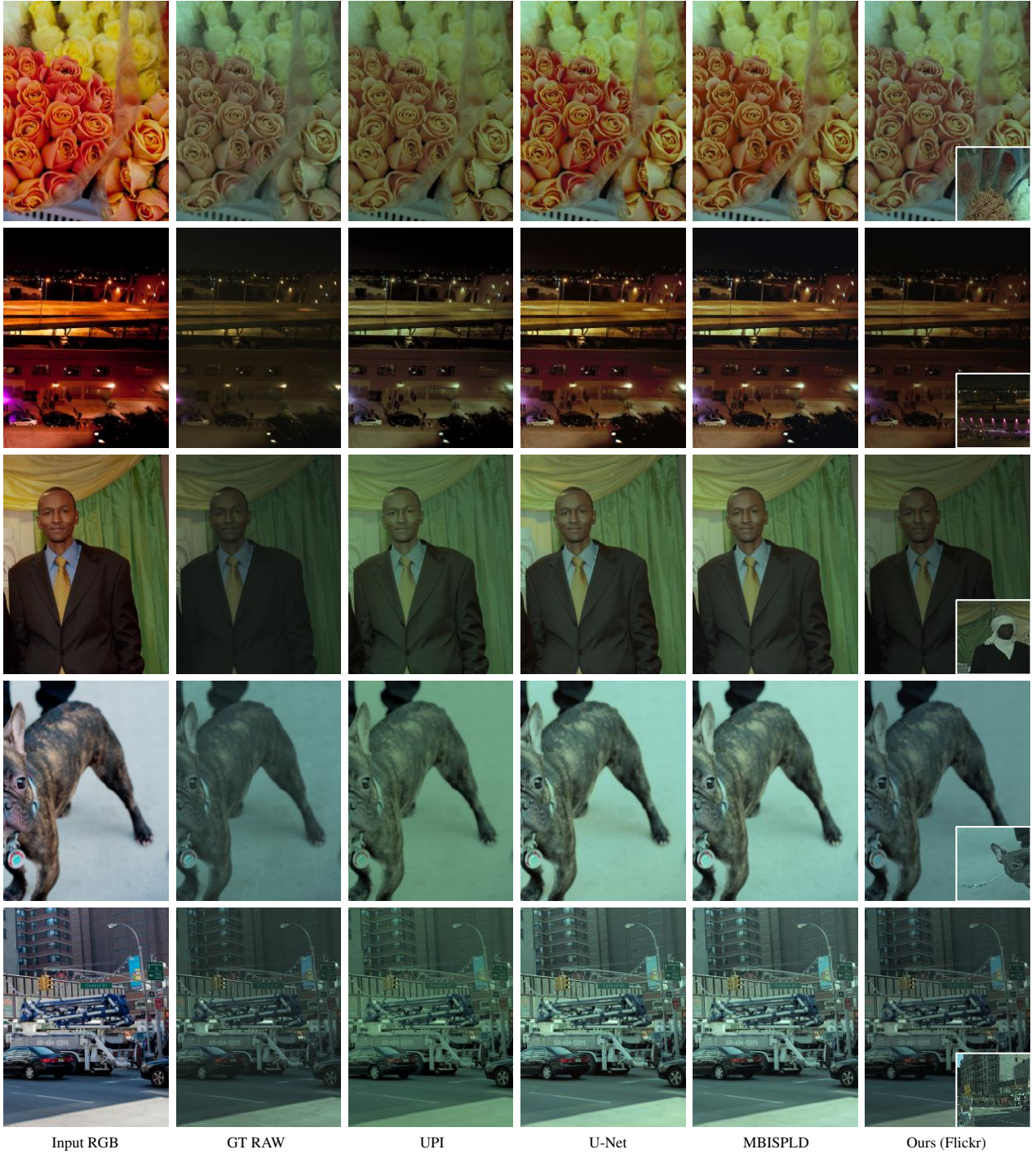


Figure 9. Qualitative RAW reconstruction results for expert-tuned Nikon D700 (Expert C). U-Net and MBISPLD were trained with the real-pairs of normal Nikon D700 (Libraw), and ours (Flickr) was trained with only the proposed pseudo-pairs (PP_{rand} and PP_{MT} for normal Nikon D700 and Flickr dataset). The small images on ours are the reference images. The gamma correction $\gamma = 2.2$ was applied to all RAW images only for visualization.



Figure 10. Qualitative RAW reconstruction results for expert-tuned Canon EOS 5D (Expert C). U-Net and MBISPLD were trained with the real-pairs of normal Canon EOS 5D (Libraw), and ours (Flickr) was trained with only the proposed pseudo-pairs (PP_{rand} and PP_{MT} for normal Canon EOS 5D and Flickr dataset). The small images on ours are the reference images. The gamma correction with $\gamma = 2.2$ was applied to all RAW images only for visualization.



Figure 11. Qualitative RAW-like conversion results for RGB images in Flickr 1 Million Dataset. Ours (Flickr) was trained with only the proposed pseudo-pairs for each RAW dataset (Nikon/Canon/SIDD/LOD dataset) and Flickr dataset. The small images on ours are the reference images, and the dataset name in the leftmost column denotes the name of the dataset from which reference images were sampled. The gamma correction with $\gamma = 2.2$ was applied to all RAW images only for visualization.



Figure 12. Qualitative RAW-like conversion results for RGB images in COCO dataset. Ours (COCO) was trained with only the proposed pseudo-pairs for each RAW dataset (Nikon/Canon/SIDD/LOD dataset) and COCO dataset. The small images on ours are the reference images, and the dataset name in the leftmost column denotes the name of the dataset from which reference images were sampled. The gamma correction with $\gamma = 2.2$ was applied to all RAW images only for visualization.